J. Fluid Mech. (1983), *vol.* 137, *pp.* 31–58
Printed in Great Britain

Fully developed periodic turbulent pipe flow. Part 1. Main experimental results and comparison with predictions

By S. W. TU
Bechtel Civil and Mineral Inc., San Francisco, California

AND B. R. RAMAPRIAN
Iowa Institute of Hydraulic Research, The University of Iowa

(Received 18 February 1982 and in revised form 19 July 1983)

The present paper is the first part of a two-part report on a detailed investigation of periodic turbulent pipe flow. In this investigation, experimental data on instantaneous velocity and wall shear stress were obtained at a mean Reynolds number of 50000 in a fully developed turbulent pipe flow in which the volumetric flow rate was varied sinusoidally with time around the mean. Two oscillation frequencies at significant levels of flow modulation were studied in detail. The higher of these frequencies was of the order of the turbulent bursting frequency in the flow, and the other can be regarded as an intermediate frequency at which the flow still departed significantly from quasi-steady behaviour. While a few similar experiments have been reported in the recent literature, the present study stands out from the others in respect of the flow regimes investigated, the magnitude of flow modulation, the detailed nature of the measurements and most importantly the identification of a relevant parameter to characterize unsteady shear flows. The present paper contains the main experimental results and comparisons of these results with the results of a numerical calculation procedure which employs a well-known quasi-steady turbulence closure model. The experimental data are used to study the manner in which the time-mean, the ensemble-averaged and the random flow properties are influenced by flow oscillation at moderate to high frequencies. In addition, the data are also used to bring out the capability and limitations of quasi-steady turbulence modelling in the prediction of unsteady shear flows. A further and more detailed analysis of the experimental data, results of some additional experiments and a discussion on the characterization of turbulent shear flows are provided in Part 2 (Ramaprian & Tu 1983).

1. Introduction

1.1. *The problem introduced*

The study of unsteady or periodic turbulent shear flows is of practical significance because of their many important applications in aerodynamics (helicopter rotor-blade dynamics), turbomachinery, biofluid flows, sediment transportation, etc. Very little information is presently available on the structure of turbulence in such flows. It is therefore essential to perform some fundamental studies on unsteady turbulent shear flows. The fully developed periodic pipe flow in which the flow rate is *forced* to vary sinusoidally with time around a mean value represents one of the simplest flows under

this category. It is therefore a natural choice for basic studies of turbulence in unsteady flows.

The problem of unsteady or periodic turbulent flow through a long circular pipe has been studied by several research workers experimentally as well as computationally. Of these, the most comprehensive experimental studies are those of Mizushina, Maruyama & Shiozaki (1973) and Mizushina, Maruyama & Hirasawa (1975). In a series of recent papers, they have reported detailed measurements of velocity, turbulence intensity and autocorrelation, at several frequencies of oscillation and at different mean Reynolds numbers. They found that imposed periodicity plays a significant role if the oscillation frequency is higher than a critical frequency. While instantaneous velocities were measured in these experiments, no specific comments were made by the authors on the effect of the imposed oscillations on the time-mean velocity profile in the flow. However, from a qualitative study of the plots of their phase-averaged velocity profiles, one gets the impression that the time-mean velocity is likely to have been affected by oscillation at the higher frequencies they studied. The distortion of the time-mean velocity was also observed by Ramaprian & Tu (1980) in their experiments on oscillatory pipe flow at transitional Reynolds number. They observed that the time-mean profile exhibited an inflexion point. In the meanwhile, Ohmi *et al.* (1976), Kita, Adachi & Hirose (1980) and Kirmse (1979) also reported experimental information on periodic pipe flow. These authors did not observe any inflexion point in the time-mean velocity profile. Instead, they concluded that the profile is essentially the same as that corresponding to steady flow at the mean Reynolds number.

Apart from the experimental data reported on oscillatory pipe flows, there has also been significant computational effort in this direction. For example, Ohmi, Kyomen & Usui (1978), Kita, Adachi & Hirose (1980) and Kirmse (1979) supplemented their experiments with numerical calculations. Others who reported computational studies of periodic pipe/channel flows are Vasiliev & Kvon (1971) and Acharya & Reynolds (1975). Most of these authors used, without much justification, simple extensions of steady-flow turbulence models to close the equations.

A review of the literature on periodic turbulent pipe flows indicates, that, while several experimental and numerical studies have been reported in the last 5 or 6 years, these studies have not led to any definite conclusions regarding the behaviour of turbulent shear flows under the influence of imposed periodic perturbation. While most of the experiments seem to indicate negligible effect of unsteadiness on the time-mean flow, there are a few experiments that indicate the contrary. Direct wall-shear-stress measurements have rarely been made, and hence the effect of unsteadiness on the behaviour of this important quantity (such as its amplitude, phase and time-mean value) is uncertain. Until very recently, studies at oscillation frequencies large enough to interact with the turbulent structure had not been made. While data are now available at high frequencies, more are required. In any case, with the exception of the work of Mizushina and coworkers, there has been no attempt to classify the periodic flows based on the frequency and amplitude of oscillation. While there are a few studies at high oscillation frequency and very small amplitude and a few others at large amplitude but very low (almost quasi-steady) frequencies there are very few detailed experiments that combine high frequencies and large amplitudes. Such conditions are often encountered in practice (e.g. aerodynamics of helicopter rotor blades). Also parameters such as Strouhal number and Stokes number have generally been used to characterize the unsteady turbulent flow. This practice, which has been borrowed from classical laminar unsteady-flow theory, has been found

to be inadequate (e.g. Ramaprian & Tu 1980) for turbulent flows. Alternative ways to characterize unsteady turbulent flows must be found. On the computational side, time-dependent calculations have been made using extensions of steady flow turbulence models in a quasi-steady manner without a careful study of their implications at different flow regimes.

1.2. *Objectives of the present study*

The earlier work of Ramaprian & Tu (1980) indicated the possibility that the time-mean behaviour of periodic turbulent pipe flow may differ from that of the quasi-steady flow at oscillation frequencies of the order of the turbulent bursting frequency. That study was performed at very low Reynolds numbers. In the present study, experiments were conducted at a much larger mean Reynolds number, *viz* 50000. Results at this Reynolds number can be directly compared with well-documented steady pipe flow data. Also, the apparatus, instrumentation and data-acquisition precedure have all been modified to improve the quality and scope of the experiments.

Detailed measurements, including instantaneous velocities (using single-channel laser-Doppler anemometry) and instantaneous wall shear stress (using flush-mounted film gauge), have been obtained at two oscillation frequencies $f_{os} = 0.5$ and 3.6 Hz. The higher frequency was large enough to interact with a significant part of the turbulent-energy spectrum. The lower frequency of oscillation can be considered to be an intermediate frequency at which the flow did not behave in a quasi-steady manner. In both these experiments the amplitude of modulation was significant enough to yield useful results. In addition to these detailed experiments, less-detailed experiments have been conducted over a larger range of oscillation frequencies. Thus the present experimental programme has been designed to cover flow regimes of practical interest and to yield detailed information on the structure of turbulence. The main experimental results are presented in this paper and are compared with the predictions obtained from a finite-difference calculation procedure based on a quasi-steady turbulence closure model. In Part 2 (Ramaprian & Tu 1983), these and additional detailed experimental results, along with the results of the numerical study, are examined to explain the structure of unsteady turbulence.

2. Experimental details

2.1. *The experimental apparatus*

The experimental apparatus is shown schematically in figure 1. The basic pipe-flow facility was originally designed and built for unsteady flow studies at transitional Reynolds numbers (see Ramaprian & Tu 1980). Some modifications were made on this system for the present study at high Reynolds numbers.

Water from the constant-head tank flows down through an inlet pipe and a curved pipe, followed by a bell-shaped contraction nozzle to a 50 mm diameter × 10 m long copper pipe. The test section where velocity measurements were made is a Plexiglas tube, 0.3 m long and 50 mm in internal diameter D. A rotating profiled sleeve driven by a regulated, geared d.c. motor controls the exit area for the water. The sleeve profile is designed to give two complete cycles of sinusoidal oscillation in discharge in one revolution. Details of the sleeve design and its drive system are described in Ramaprian & Tu (1982). Two sleeves were used – one designed for an amplitude of 15% at $f_{os} = 3.6$ Hz and the other for an amplitude of 65% at 0.5 Hz. The performance of these sleeves is seen from figure 2, which shows the actual modulations

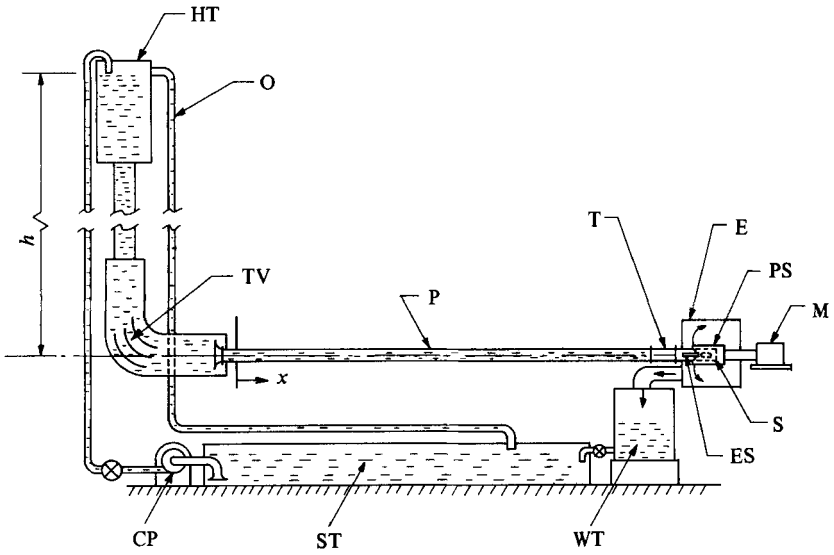

FIGURE 1. Layout of the experimental apparatus: HT, head tank; O, overflow pipe; TV, turning vanes; P, 50 mm diameter copper pipe; T, test section; E, Plexiglas enclosure; PS, profiled sleeve; M, geared motor; S, slotted brass cylinder; ES, exit slots; WT, weigh tank; ST, sump tank; CP, circulating pump; $h \approx 4$ m; x = distance from first pressure tap.

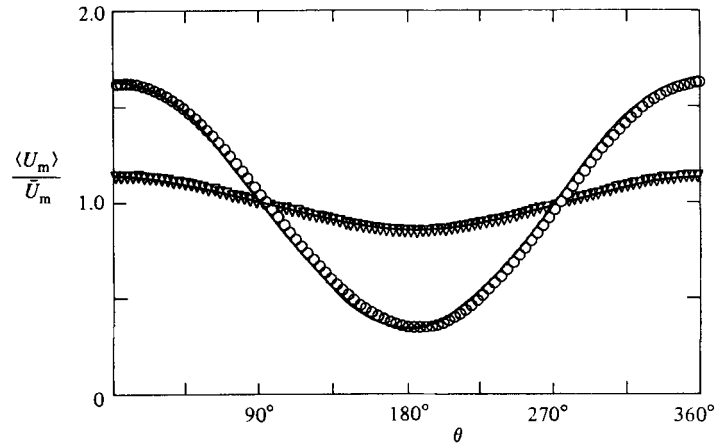

FIGURE 2. Discharge modulation obtained with the two sleeves: ▽, 3.6 Hz; ○, 0.5 Hz; ——, exact sine wave.

in discharge (or equivalently in cross-sectional average velocity $\langle U_m \rangle$) obtained with these sleeve profiles. It is seen that the modulations are very nearly sinusoidal in both cases.

2.2. *Instrumentation and calibration*

Wall static pressure P_w distribution along the pipe in steady flow was measured using the static pressure taps and an inverted U-tube water manometer. Pressure measurements were not made in unsteady flow owing to instrumentation difficulties. The time-averaged flow rate and hence the time-mean cross-sectional average velocity $\bar{U}_m$ (with an uncertainty of less than 0.5 %) was measured using the weigh tank and

a stop watch. Instantaneous velocity in the axial direction was measured using frequency-shifted laser-Doppler anemometry (LDA). Owing to the finite length of the measuring-volume, which is of the order of 1.6 mm in the radial direction, there is an uncertainty in the determination of the effective distance y from the wall. In order to reduce this difficulty and ensure consistency, the 'zero' of the traverse and hence the effective measurement location were fixed by matching the discharge computed from the integration of the velocity profiles with the discharge measured using the weigh tank. The surface shear stress τ_w was measured using a DISA constant-temperature hot-wire anemometer and a flush-mounted quartz-coated film probe. An overheat ratio of 1.05 was used. The gauge was calibrated *in situ* in steady flow at several Reynolds numbers immediately before and after its use in the unsteady flow. The details of instrumentation and calibration are given in Ramaprian & Tu (1982).

2.3. *Ensemble averaging and definitions*

An ensemble-averaging procedure was used in the present study for the analysis of unsteady turbulent flow. This procedure is identical with that used in the earlier work (Ramaprian & Tu 1980). In this procedure, any instantaneous quantity Φ (Φ representing the longitudinal velocity U or the radial velocity V) at time t, at a radial location r, and a phase position θ in the oscillation cycle is written as

$$\begin{aligned}\Phi(r,\theta,t) &= \overline{\Phi}(r)+\Phi_p(r,\theta)+\phi(r,\theta,t)\\ &= \langle\Phi\rangle(r,\theta)+\phi(r,\theta,t),\end{aligned} \tag{1}$$

where $\overline{\Phi}$ is the (long) time-mean quantity $\overline{U}$ or $\overline{V}$, $\langle\Phi\rangle$ is the deterministic (ensemble-averaged) quantity $\langle U\rangle$ or $\langle V\rangle$, Φ_p is the purely periodic part U_p or V_p, and ϕ is the turbulent (random) quantity, u or v. Note that $\overline{V}$, V_p and $\langle V\rangle$ are zero in the fully developed periodic pipe flow. The r.m.s. ensemble-averaged values u'_p and v'_p of turbulent velocity fluctuations are defined as

$$\phi'_p(r,\theta) = (\langle\phi^2(r,\theta,t)\rangle)^{\frac{1}{2}} = [\langle\{\Phi(r,\theta,t)-\langle\Phi\rangle(r,\theta)\}^2\rangle]^{\frac{1}{2}}, \tag{2}$$

and the ensemble-averaged 'Reynolds shear stress' can be conceptually defined as

$$\begin{aligned}-\langle uv\rangle(r,\theta) &= -[\langle\{U(r,\theta,t)-\langle U\rangle(r,\theta)\}\{V(r,\theta,t)-\langle V\rangle(r,\theta)\}\rangle]\\ &= -[\langle\{U(r,\theta,t)-\langle U\rangle(r,\theta)\}\,V(r,\theta,t)\rangle].\end{aligned} \tag{3}$$

The conventional r.m.s. turbulent intensities u' and v' (on long-time-average basis) are defined as

$$\phi'(r) = \left[\frac{1}{2\pi}\int_0^{2\pi}\phi'^2_p(r,\theta)\,\mathrm{d}\theta\right]^{\frac{1}{2}}, \tag{4}$$

and the conventional Reynolds shear stress is defined as

$$-\overline{uv} = \frac{1}{2\pi}\int_0^{2\pi} -\langle uv\rangle(r,\theta)\,\mathrm{d}\theta. \tag{5}$$

The (long) time-mean, ensemble-averaged and turbulent components mentioned above were obtained from the instantaneous values using a digital data-acquisition and processing scheme. Taking advantage of the periodic nature of the flow, ensemble averages were obtained by treating successive cycles as independent realizations. Hence instantaneous values Φ obtained at identical phase positions θ in a large number of cycles were averaged to obtain $\langle\Phi\rangle$ and hence $\overline{\Phi}$, Φ_p and ϕ'_p. A total of 1000 cycles were used in this ensemble or 'phase-averaging' procedure. Details are

provided in Ramaprian & Tu (1982). A similar procedure was used to obtain the ensemble average $\langle \tau_w \rangle(\theta)$ and the time-mean $\bar{\tau}_w$ values of the wall shear stress from the instantaneous output of the shear-stress gauge. Turbulent intensities were not computed in this case since there was doubt about the dynamic response of the gauge at high frequencies.

Unfortunately, since a single-channel LDA was used in the present experiments, it was not possible to make *direct* measurements of the r.m.s. intensities v'_p, v' and the Reynolds shear stresses $-\langle uv \rangle$ and $-\overline{uv}$. However, it is possible (see Ramaprian & Tu 1980) to compute $\langle uv \rangle(r, \theta)$ from the integral momentum equation, after expressing the pressure gradient in terms of the ensemble-averaged velocity $\langle U \rangle$ and wall shear stress $\langle \tau_w \rangle$ in the following form:

$$-\langle uv \rangle(r,\theta) = \frac{1}{r}\int_0^r \frac{\partial}{\partial t}[\langle U(r,\theta)\rangle - \langle U_m\rangle(\theta)]\, r_1\, dr_1 + \frac{2\langle \tau_w\rangle(\theta)\, r}{\rho D} - \nu \frac{\partial \langle U\rangle(r,\theta)}{\partial r}. \quad (6)$$

The right-hand side of (6) was evaluated using measured velocity and wall-shear-stress data. The process required differentiation with respect to time and integration across the pipe, both of which were performed numerically on a computer. The velocity–time data were smoothed digitally in order to reduce the numerical noise in differentiation. The accuracy of the entire procedure has been established in connection with the earlier work of Ramaprian & Tu (1980). It is estimated that the values of $\langle uv \rangle$ obtained in this manner are accurate to 10% in the present cases.

2.4. *Experimental details*

Three series of experiments were performed. These are

(i) steady-flow experiments at several Reynolds numbers (series 1);

(ii) detailed unsteady-flow experiments at oscillation frequencies of 3.6 Hz and 0.5 Hz (series 2);

(iii) unsteady-flow experiments over a range of oscillation frequencies (series 3).

Steady flow measurements were made for discharge, pressure drop and velocity distribution across the pipe at five Reynolds numbers Re, namely 20700, 38860, 49420, 71790 and 79800. The Reynolds-number range studied in these experiments corresponds roughly to the extreme values of Reynolds number reached during an oscillation cycle in the unsteady flow experiments. Some of these experiments were repeated several times. The scatter in the results was less than 1% for mean velocity and less than 5% for turbulent intensity.

The pressure-drop measurements confirmed the validity of the Blasius friction formula for the friction factor λ:

$$\lambda = 0.4265 Re^{-\frac{1}{4}}. \quad (7)$$

This fact was made use of in the quick calibration of the shear-stress gauge since the gauge can be calibrated by simply measuring the discharge of various operating conditions.

In the second series of experiments, the flow at a mean Reynolds number of 5×10^4 was oscillated at the desired frequency (3.6 Hz/0.5 Hz) using the appropriate sleeve for each frequency. The higher frequency of 3.6 Hz roughly corresponds to the turbulent bursting frequency f_b in the mean flow, estimated from the relation $U_m/f_b D = 5$ suggested (for boundary layers) by Rao, Narashimha & Badri Narayanan (1971). The lower frequency of 0.5 Hz can be considered to be an 'intermediate' frequency. The third series of experiments and their results are described in Part 2.

Velocity measurements were made at about 20 points across the pipe. Data were

sampled and collected two hundred times per sleeve revolution (or one hundred times per oscillation cycle) over 1000 cycles. These data were later processed for obtaining the distributions of $\overline{U}$, U_p, u'_p and u' across the pipe. The first set of experiments (at 3.6 Hz) were repeated several times to determine the repeatability of the results. The scatter in the results was again found to be less than 1 % for mean quantity and less than 5% for turbulent intensity. Wall-shear-stress measurements were made independently of the velocity measurements and were obtained by sampling at 100 phase positions in a cycle and averaging over 300 cycles. From the instantaneous wall-shear-stress data, long-time averaged and ensemble-averaged values were obtained.

3. Results and discussion

3.1. *General*

The experimental results will now be presented and discussed. In the interest of brevity, only typical figures are introduced. More details, including a complete set of tabulated experimental data, are available in Ramaprian & Tu (1982). The experimental results of series 2 are compared with the results obtained from a numerical solution of the ensemble-averaged unsteady equations of momentum and turbulent kinetic energy using a finite-difference method. The turbulence model used for closure of the equations is the ensemble-averaged version of the well-known Prandtl-energy model. The model is used in the form

$$\langle \nu_t \rangle \propto \langle q^2 \rangle^{\frac{1}{2}} l[1-\exp(-c_3 \langle q^2 \rangle^{\frac{1}{2}} y/\nu)], \tag{8}$$

where $\langle \nu_t \rangle$ is the ensemble-averaged eddy viscosity, $\langle q^2 \rangle$ is twice the ensemble-averaged turbulent kinetic energy ($\langle u^2 \rangle + \langle v^2 \rangle + \langle w^2 \rangle$), ν is the viscosity and c_3 is a model constant. The lengthscale l is assumed to be independent of time, and is specified as

$$l = \frac{4R}{30}(1-\eta)^3, \tag{9}$$

where R is the radius of the pipe and $\eta = y/R$. The turbulence closure model as well as the model for the turbulent dissipation (with correction for low-Reynolds-number effects near the wall) and the model constants are all identical with those used by Acharya & Reynolds (1975). These physical models are, in fact, the same as are generally used for steady turbulent flows. One can thus regard the present approach as 'quasi-steady' modelling. The finite-difference grid was extended up to the wall, and hence there was no need to use the so-called 'wall-functions' (see e.g. Patankar 1967). The details of the calculation procedure are described in Ramaprian & Tu (1982). In the present paper and in Part 2, only some results of the calculation which are relevant for comparison with the measurements are presented.

3.2. *Steady-flow measurements*

Figure 3 shows the mean-velocity profiles across the pipe in the usual wall-layer coordinates $U^+(= \overline{U}/\overline{U}_*)$ and $Y^+(= y\overline{U}_*/\nu)$. It is seen that all the steady-flow profiles follow the universal log law reasonably well. Nevertheless, in the wall region ($Y^+ \leqslant 70$) the measurements seem to be inaccurate. For example, they seem to be about 15–20 % higher than the measurements of Laufer (1954) shown by the shaded lines. This is due to the sharp change of velocity across the LDA measuring volume, which has a length of about 1.6 mm in the radial direction. The measured values

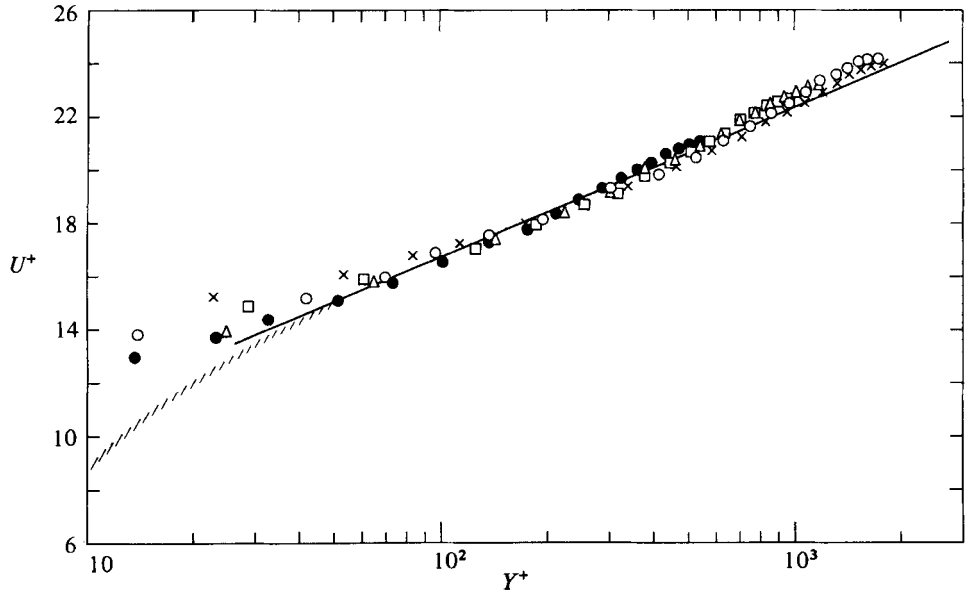

FIGURE 3. Mean-velocity distributions in the wall-layer coordinates at various Reynolds numbers in steady pipe flow: ×, $Re = 79800$; ○, 71790; △, 49420; □, 38860; ●, 20700; ////, data of Laufer (1954) at $Re = 50000$; ——, $U^+ = 2.44 \ln Y^+ + 5.5$.

therefore actually represent an average over this length. This is a shortcoming with the use of LDA near the wall in the present experiments. Hence in the region $Y^+ \leqslant 70$ the present measurements can be considered to have uncertainties of about 20% or higher. The distributions of the longitudinal turbulent intensity u' were also obtained at various Reynolds numbers. It was found that the data at all Reynolds numbers except the lowest, namely $Re = 20700$, were in good agreement with the data of Laufer (1954). The experiments were repeated several times and the data were found to be reproducible within a scatter of 5%. These data can be used for comparison with those corresponding to truly periodic flows at finite oscillation frequencies.

3.3. *Quasi-steady-flow results*

3.3.1. *General*

The steady-flow results described in §3.2 can also be regarded as results obtained in periodic flow at an infinitely low frequency of imposed oscillation. Such an unsteady flow will be called quasi-steady flow. In such a flow, all the flow properties such as mean velocity, turbulence intensity and wall shear stress at any phase position θ during the oscillation cycle will be equal to the corresponding properties in steady flow at the same instantaneous Reynolds number. By averaging the results for steady flow at several Reynolds numbers in the appropriate range, one can recover the information on time-averaged flow properties for quasi-steady flow with a given amplitude of modulation. Because of nonlinear effects this average will not strictly be equal to the flow properties at the average Reynolds number of the quasi-steady flow. The difference between the two may become significant at large amplitudes of modulation. If one has to study the effect of imposed periodicity at a *finite* frequency, one has to compare the actual unsteady-flow results with the corresponding results for a hypothetical *quasi-steady flow* of the same amplitude and same mean Reynolds number and not with the results for steady flow at the same average Reynolds

number. This point has been consistently ignored by all research workers so far. While, in many cases, this has not been serious since the amplitudes of modulation were very small, there have been a few cases (where large amplitudes were studied) where ignoring of this aspect cannot be justified. In this section, some of the results for quasi-steady flow are developed from steady-flow results.

3.3.2. *Time-mean wall shear stress in quasi-steady flow*

As mentioned earlier, Blasius' formula in the form of (7) is valid for steady flow in the Reynolds-number range of the present study, as confirmed by pressure-drop measurements. The magnitude of the wall shear stress is thus given by

$$\left|\frac{\tau_w}{\rho}\right| = \tfrac{1}{8}\lambda \bar{U}_m^2. \tag{10}$$

Let us assume that the cross-sectional average velocity varies with time according to

$$\langle U_m \rangle = \bar{U}_m(1+\gamma_{U_m}\cos\omega t), \tag{11}$$

where γ_{U_m} represents the relative amplitude of oscillation of $\langle U_m \rangle$. If the flow is oscillating at infinitely small frequency, (7) can be assumed to be valid at every instant. Substituting (11) into (7) and averaging over one period of oscillation, one gets the time-mean wall shear stress $\bar{\tau}_w$ as

$$\frac{\bar{\tau}_w}{\tau_w|_{\bar{R}e}} = \frac{1}{2\pi T}\int_0^{2\pi}(1+\gamma_{U_m}\cos\omega t)^{\frac{7}{4}}\,\mathrm{d}t = g_1(\gamma_{U_m}), \tag{12}$$

where $\tau_w|_{\bar{R}e}$ represents the wall shear stress at time-mean Reynolds number $\bar{R}e(=\bar{U}_m D/\nu)$, and T represents the time period of one cycle ($=1/f_{os}$, f_{os} being the oscillation frequency). The quantity g_1, which is a function of γ_{U_m}, has values of about 1.02 and 1.15 respectively for modulation amplitudes of 15 % and 64 % used in the present unsteady-flow experiments.

3.3.3. *The log law for the time-mean quasi-steady flow*

It is also interesting to perform the same analysis for the well-known universal log law. As already shown in figure 3, the steady-flow measurements follow this law reasonably well over the Reynolds-number range 20000–70000. Thus, for quasi-steady oscillation in this range of Reynolds numbers, we assume

$$\frac{\langle U \rangle}{\langle U_* \rangle} = A\ln\frac{y\langle U_* \rangle}{\nu} + B, \tag{13}$$

where A and B are the same (universal) constants as in steady flow (namely $A = 2.44$, $B = 5.5$).

Integrating (13) over a complete cycle using Blasius' friction formula (7) and (12), we get

$$\begin{aligned}\frac{\bar{U}}{\bar{U}_*} &= \left[A\ln\left(\frac{y\bar{U}_*}{\nu}g_3\right)+B\right]\frac{1}{g_1 g_2^{\frac{1}{2}}}\\ &= A\left[\ln\left(\frac{yU_*}{\nu}g_3\right)^{1/g_1 g_2}\exp\left\{\left(\frac{1}{g_1 g_2^{\frac{1}{2}}}-1\right)\frac{B}{A}\right\}\right]+B\\ &= A\ln Y^{++}+B,\end{aligned} \tag{14}$$

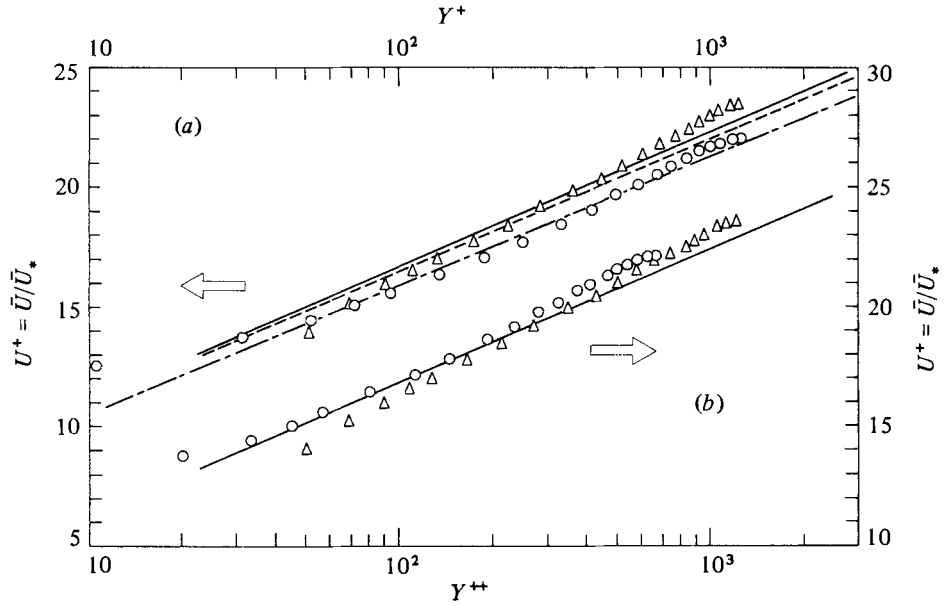

FIGURE 4. Time-mean velocity profiles in the wall-layer coordinates. (*a*) Conventional coordinates U^+ *vs.* Y^+: △, 3.6 Hz ($\gamma_{U\mathrm{m}} = 15\,\%$): ○, 0.5 Hz ($\gamma_{U\mathrm{m}} = 64\,\%$); – – –, quasi-steady flow with $\gamma_{U\mathrm{m}} = 30\,\%$ (14); — — —, quasi-steady flow with $\gamma_{U\mathrm{m}} = 60\,\%$ (14); ——, $U^+ = 2.44 \ln Y^+ + 5.5$. (*b*) Modified coordinates U^+ *vs.* Y^{++}: △, 3.6 Hz; ○, 0.5 Hz; ——, $U^+ = 2.44 \ln Y^{++} + 5.5$.

where

$$\bar{U}_* = \left(\frac{\bar{\tau}_w}{\rho}\right)^{\frac{1}{2}},$$

$$g_2 = \frac{1}{2\pi T}\int_0^{2\pi} (1+\gamma_{U\mathrm{m}}\cos\omega t)^{\frac{1}{8}}\,\mathrm{d}t, \tag{15}$$

$$g_3 = \frac{1}{g_1^{\frac{1}{2}}}\left[\frac{1+(1-\gamma_{U\mathrm{m}}^2)^{\frac{1}{2}}}{2}\right]^{\frac{7}{8}}. \tag{16}$$

The time-averaged log law for quasi-steady periodic flow is therefore displaced vertically from the universal log law for steady flow by the amount

$$\frac{A}{g_1 g_2^{\frac{1}{2}}}\ln g_3 + \left(\frac{1}{g_1 g_2^{\frac{1}{2}}} - 1\right)B$$

and its slope is also changed by a factor of $1/g_1 g_2^{\frac{1}{2}}$. This is seen from figure 4, where typical results are shown for two hypothetical quasi-steady flows of amplitudes 30 and 60 %. Therefore, for describing the mean velocity distribution in time-averaged wall-layer coordinates, it is necessary to use Y^{++} (defined by (14)) instead of the usual $Y^+ (= yU_*/\nu)$, in order to remove the amplitude effect.

3.3.4. *Time-mean velocity profile in quasi-steady flow*

Since the velocity profile in pipe flow is Reynolds-number dependent, the time-mean velocity profile in quasi-steady flow will be different from that in steady flow at the mean Reynolds number. The time-mean velocity profile $\bar{U}(y)$ in quasi-steady flow at a prescribed amplitude can be calculated by averaging the profiles $U(r, Re)$ obtained

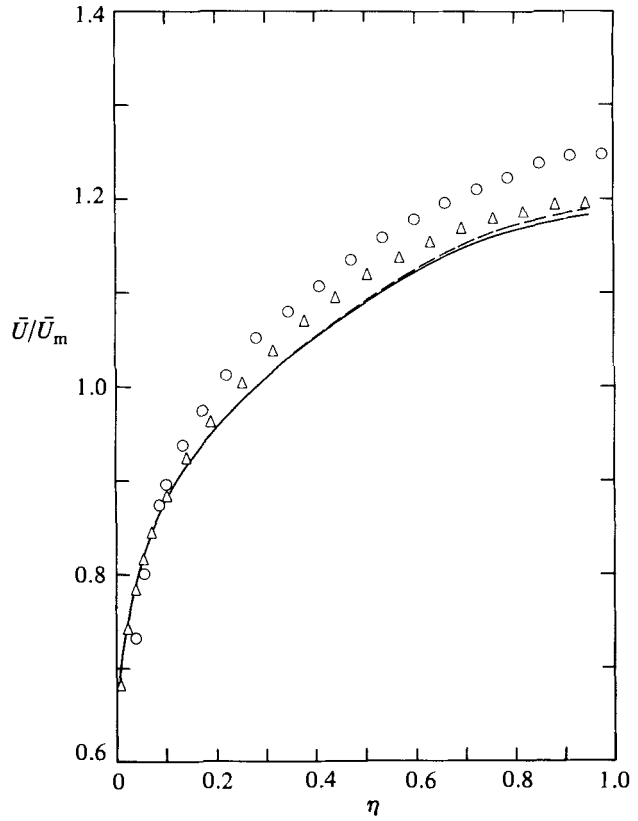

FIGURE 5. Time-mean velocity profiles in unsteady and quasi-steady flows at $\bar{R}e \approx 49400$: ○, 3.6 Hz ($\gamma_{U_m} = 15\,\%$); △, 0.5 Hz ($\gamma_{U_m} = 64\,\%$); ---, quasi-steady flow ($\gamma_{U_m} = 30\,\%$); ——, quasi-steady flow ($\gamma_{U_m} = 60\,\%$). The velocity profile in steady flow at the time-mean Reynolds number is indistinguishable from the dashed line.

experimentally in steady flow at different Reynolds numbers over the complete range of Reynolds numbers as

$$\bar{U}(r) = \frac{1}{\Delta Re}\int_{Re_{\min}}^{Re_{\max}} U(y, Re)\,\mathrm{d}Re, \tag{17}$$

where $\Delta Re = Re_{\max} - Re_{\min}$ is the range of the Reynolds number Re in steady flow.

The time-mean velocity profiles obtained for two typical quasi-steady amplitudes, 30 and 60 %, are shown in figure 5. The profile for 30 % amplitude is practically indistinguishable from the profile at the time-mean Reynolds number. The time-mean velocity profile for 60 % amplitude, however, shows a slight change from the velocity profile at the mean Reynolds number. The time-mean velocity is seen to be slightly lower than in steady flow at mean Reynolds number, near the centreline. To compensate for this, the quasi-steady flow should have a slightly larger velocity than the steady flow near the wall. This was indeed found to be true though it is not clearly seen in figure 5.

3.3.5. *Time-mean turbulence intensity in quasi-steady flow*

Lastly, the time-mean value of the longitudinal turbulent intensity u' in quasi-steady periodic flow can be defined as

$$u'^2(y) = \frac{1}{\Delta Re}\int_{Re_{\min}}^{Re_{\max}} u_p'^2(y, Re)\,\mathrm{d}Re, \tag{18}$$

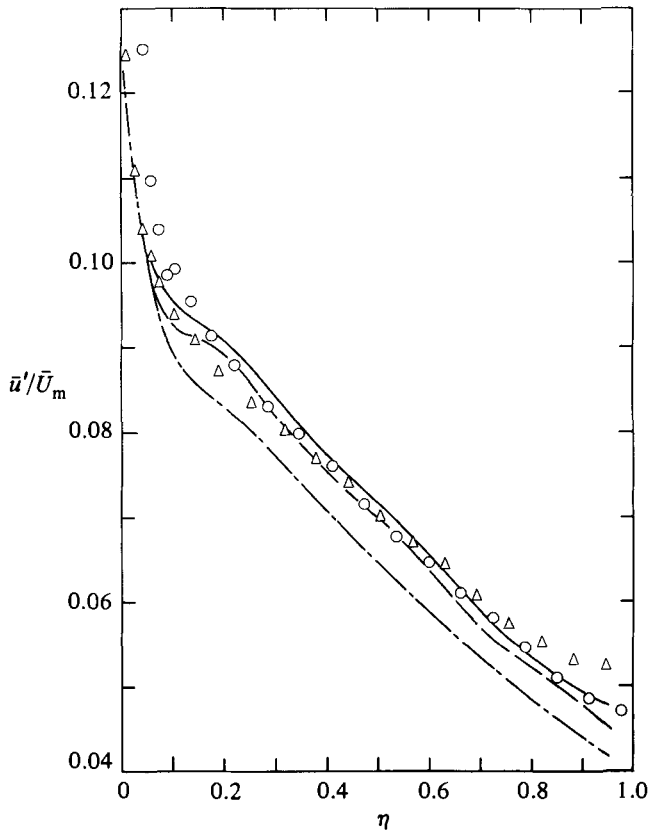

FIGURE 6. Time-mean distributions of the longitudinal turbulence intensity in unsteady and corresponding quasi-steady flows at $Re = 49400$: ○, 3.6 Hz ($\gamma_{U_m} = 15\,\%$); △, 0.5 Hz ($\gamma_{U_m} = 64\,\%$); – – –, quasi-steady flow ($\gamma_{U_m} = 30\,\%$); ——, quasi-steady flow ($\gamma_{U_m} = 60\,\%$); — — —, steady flow at $Re = 49400$.

where u'_p is the turbulence intensity at any Reynolds number Re. The time-mean distributions for two representative amplitudes, 30 and 60 %, as well as for steady flow at mean Reynolds number (0 % amplitude), are shown in figure 6. These were obtained from the steady-flow data described earlier. Significant effect of the oscillation amplitude is seen especially between 0 and 30 %. The amplitude effect decreases as the amplitude is further increased. Some of these differences can be suppressed if $\bar{U}_*$ is used as the scaling velocity instead of $\bar{U}_m$, but figure 6 is adequate to provide the basis for studying the effect of oscillation frequency in the periodic flow.

3.4. *Unsteady-flow measurements*

3.4.1. *Time-mean velocity distribution*

Figure 5 also shows the distribution of the time-average velocity $\bar{U}$ across the pipe for the two periodic flows at oscillation frequencies $f_{os} = 3.6$ Hz and $f_{os} = 0.5$ Hz respectively, so that these can be compared with the time-mean velocity profile for quasi-steady flow of corresponding amplitude in each case. It is observed that the time-mean velocity in the unsteady flow does show a difference from that in quasi-steady flow at both the frequencies. At $f_{os} = 3.6$ Hz (with amplitude 15 %) the

time-mean velocity in unsteady flow is higher by about 5 % near the centreline when compared to that in the corresponding quasi-steady flow. For 0.5 Hz the difference is smaller, yet is still higher than quasi-steady velocity near the centreline. A corresponding decrease in the velocity relative to the quasi-steady mean velocity can be seen in the region near the wall. Again the contrast is more clearly seen at the oscillation frequency of 3.6 Hz, which is of the same order as the turbulent bursting frequency. This finding is in agreement with the earlier work (Ramaprian & Tu 1980). It is particularly significant that it is in contradiction with most of the published results that the authors are aware of. However, these latter experiments generally suffer from several limitations that have prevented the detection of the effect of imposed oscillations on the time-mean flow. For example, the oscillation frequencies used in these experiments were very low compared with the turbulent bursting frequency. Also the oscillation amplitude in many cases was too small (5 % or less) to produce differences distinguishable beyond the experimental scatter. In some experiments, large amplitudes and high frequencies were studied (e.g. Mizushina *et al.* 1973, 1975; Kita *et al.* 1980). In these experiments oscillation amplitudes of 40 % or more and oscillation frequencies comparable to the bursting frequency have been studied. Significant interaction between imposed unsteadiness and the turbulence structure can be expected to have been present in these experiments. However, quantitative study of the time-mean velocity was not made by Mizushina *et al.*, even though they seem to have had the necessary data. The data of Kita *et al.* do, in fact, seem to show small but definite effect of oscillation on the time-mean velocity. These authors, however, stated that the time-mean velocity of the unsteady flow agreed with that corresponding to steady flow at the mean Reynolds number, a statement which cannot be correct (as already shown in the previous section) since the amplitude of oscillation in their study was as high as 50 %.

To summarize, it can be stated that there is definite evidence from the present experiments as well as from the earlier experiments of Ramaprian & Tu (1980) that, at interactive frequencies of oscillation and large enough amplitudes, the time-mean velocity profile in periodic flow is affected by the imposed unsteadiness and differs slightly from that corresponding to a quasi-steady flow with the same amplitude of modulation.

Figure 4(*a*) also shows the time-mean velocity distributions in the wall-layer coordinates (U^+ *vs.* Y^+) for the two periodic flows studied and for the quasi-steady flows corresponding to each case. Significant differences are seen among the four profiles with respect to the existence of a semilogarithmic velocity distribution in the fully turbulent wall region. Figure 4(*b*) shows these distributions plotted in the modified wall-layer coordinates U^+ and Y^{++} of (14). In this figure the effect of oscillation amplitude is removed, and the full line represents the quasi-steady periodic flow at all amplitudes. The two sets of experimental data show the effect of the frequency of oscillation. It is seen that the time-mean velocity does not follow the universal log law for either of the two oscillation frequencies. No particular trend is recognizable in the relationship of the distortion of the velocity profile to the oscillation frequency. In any case, the present observations do not support the observations/assumptions of many previous investigators (e.g. Binder & Kueny 1981; Cousteix, Houdeville & Javelle 1980) that the universal log law is valid in unsteady flow. The present observation also indicates that use of the universal log-law assumption for the measurement of wall shear stress by the above authors or the use of quasi-steady wall functions (as was done by Cousteix *et al.*) in the prediction of unsteady turbulent boundary layers are not justified. The observation of a universal

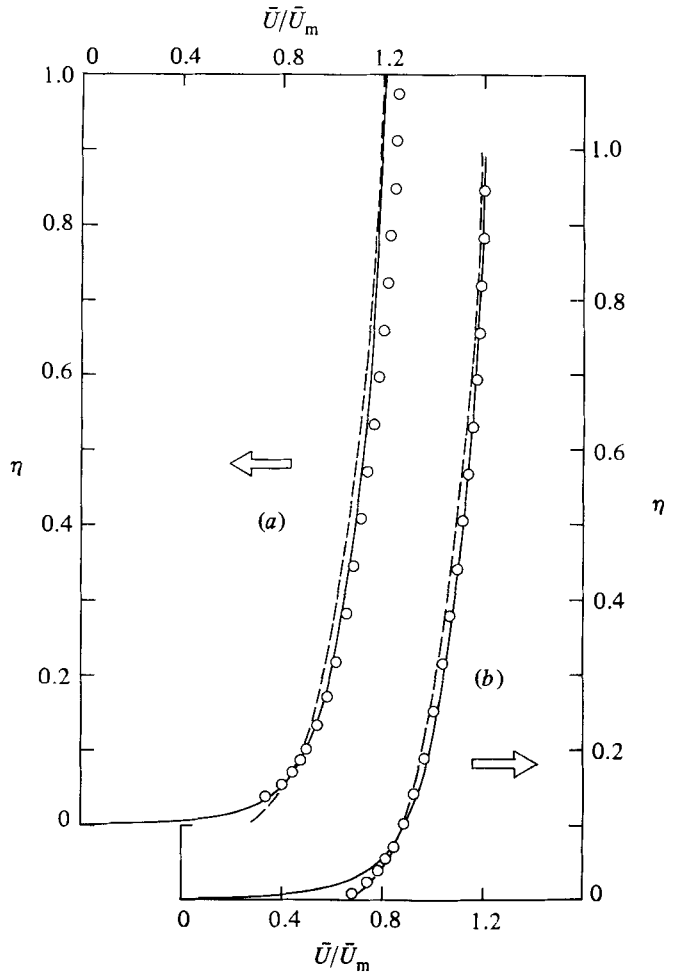

FIGURE 7. Time-mean velocity profile in unsteady flow – comparison with quasi-steady flow and with prediction: (*a*) $f_{os} = 3.6$ Hz; (*b*) $f_{os} = 0.5$ Hz: ○, unsteady-flow data; ----, quasi-steady flow of the same amplitude γ_{Um}; ——, numerical prediction.

log law by Binder & Kueny in the periodic flow is presumably due to a combination of reasons, namely a very low amplitude of oscillation (less then 5%), use of the log-law assumption to determine $\bar{U}_*$ and experimental errors and scatter being indistinguishable from weak trends.

The time-mean velocity distributions measured in the present experiments are compared in figures 7(*a*), (*b*) with the predictions obtained from the numerical analysis. As already mentioned, numerical calculations were performed using, in each case, the exact pressure-gradient variation with time corresponding to the particular experiment. First, it is seen that there is a slight difference between the unsteady flow predictions and the quasi-steady flow. A careful examination indicates that this difference is almost independent of the oscillation frequency of the unsteady flow. It was, in fact, found to be present in the predictions for steady pipe flow also (see Ramaprian & Tu 1982). It is therefore intrinsic to the method and the model since the model constants have been chosen directly as used by Acharya & Reynolds (1975) without making any effort to fine-tune them.

The predicted distribution is, however, seen to be different from the experimental measurement at 3.6 Hz but not significantly different from the measured distribution at 0.5 Hz. Figure 7(*a*) shows that, specifically at 3.6 Hz, the measured velocity is larger than predicted by about 5 % near the centreline of the pipe. An opposite trend is indicated near the wall, as expected. However, because of the relatively larger uncertainty in the LDA measurements very near the wall (say $Y^+ < 70$), it is safer to restrict the comparisons to the region $Y^+ > 70$, where the accuracy of the measurement is equal to or better than 1 %. Based on comparisons in this region, one can conclude that the calculation method based on the assumed quasi-steady turbulence model predicts negligible effect of oscillation frequency on the time-mean flow and thus the predictions deviate from measurement especially at high or interactive oscillation frequencies.

3.4.2. *Time-mean turbulence intensity distribution*

Figure 6 also shows the distribution of time-mean turbulence intensity u' at two frequencies in the unsteady flow. Comparing the unsteady-flow data with those of the quasi-steady flow at approximately similar amplitude, it is noticed that at 3.6 Hz ($\simeq$ 15 % amplitude) the distribution reasonably agrees with that in quasi-steady flow (30 % amplitude) in the core region within the experimental accuracy of ± 2 %. Near the wall, however, the measured values seem to be slightly larger than in quasi-steady flow. Unfortunately quasi-steady data for $\gamma_{U_m} = 15$ % were not obtained, but the present comparison is adequate to indicate the trends. At 0.5 Hz ($\approx$ 64 % amplitude), the unsteady flow exhibits nearly the same intensities as the quasi-steady flow in the region $0.1 < \eta < 0.6$, but higher intensities than quasi-steady flow for $\eta > 0.6$. The difference between the unsteady and quasi-steady flow in this case is about 10 % near the centreline, and is clearly much larger than the experimental uncertainties of ± 2.5 %. Binder & Kueny (1981), based on their experimental data at high frequency of oscillation, concluded that turbulent intensity remains unchanged in unsteady flow. Their amplitude, however, was less than 5 %, and this made any change in intensities extremely hard to detect amidst their experimental scatter. Some of the experiments on oscillating turbulent boundary layers (Cousteix *et al.* 1981) at very low frequencies of oscillation also seem to have indicated negligible effect of oscillation on time-mean intensity. These authors have not, however, based their comparisons on the appropriate quasi-steady flow.

3.4.3. *Ensemble-averaged velocity distributions*

Figure 8 gives the distributions of ensemble-(phase-)averaged velocities $\langle U \rangle$ across the pipe at several phase positions in one cycle. The phase angles are referred to the instant when the cross-sectional-average velocity attains the maximum value. Velocity distributions across the pipe at phase intervals of approximately 45° are presented in these figures. The normalizing velocity used is the time-mean cross-sectional-average velocity, $\overline{U}_m$. Figures 8(*a*, *b*) show the measurements at 3.6 Hz, and figures 8(*c*, *d*) present the results for 0.5 Hz. For the sake of clarity, the deceleration ($\theta = 0°$–$180°$) and acceleration ($\theta = 180°$–$360°$) periods are shown separately. It can be seen that, at 3.6 Hz, the velocity profiles across most of the pipe look similar to one another at all phase positions except for a shift upwards or downwards as the cross-sectional velocity varies with time. On the other hand, at 0.5 Hz, the flow oscillation is seen to affect the shape of the velocity profiles across most of the pipe. The distortion is, in fact, large enough to cause inflexion points to appear in the profiles at some phase positions. Some of these velocity profiles look similar to the

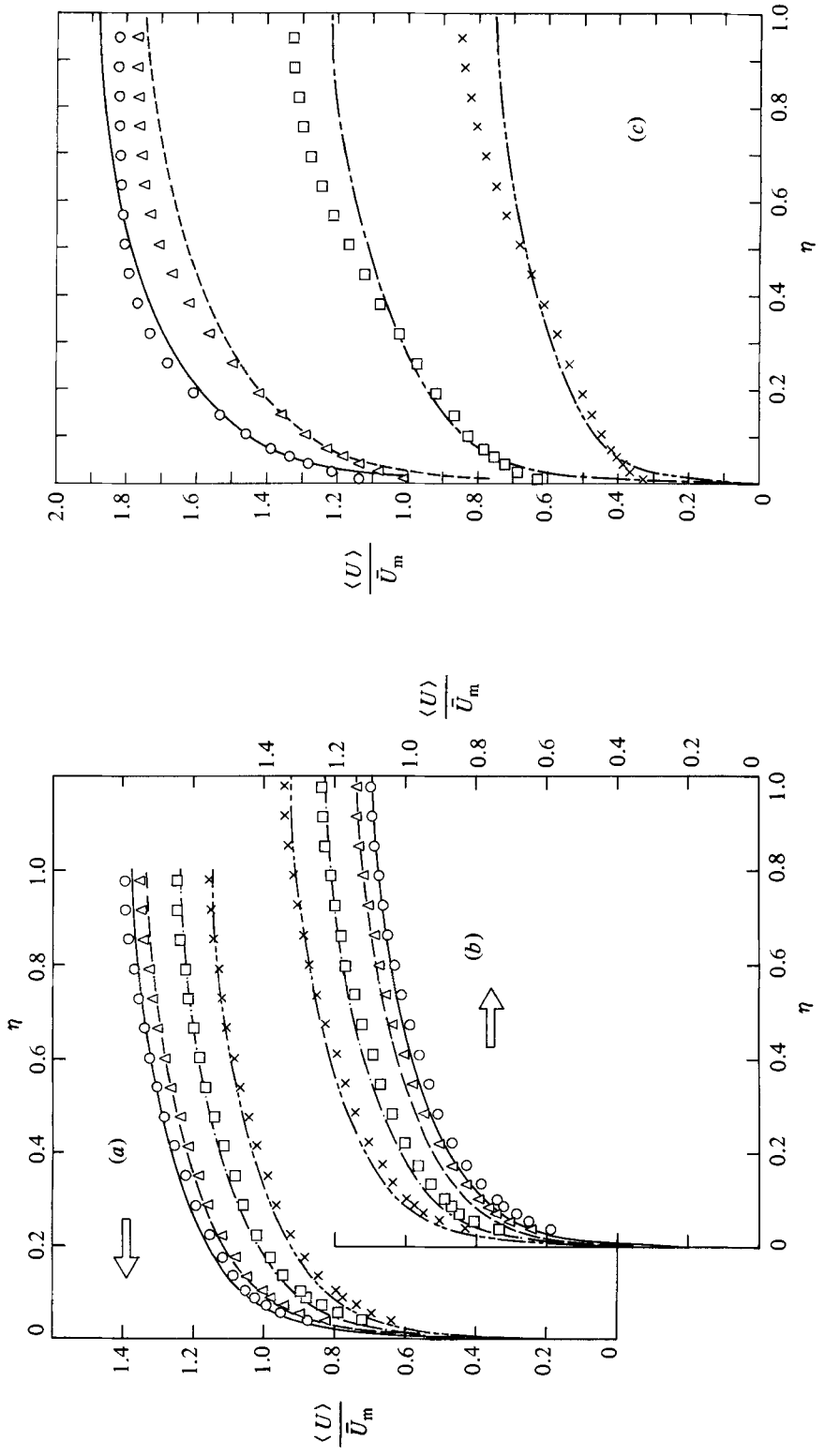
(a)
(b)
(c)
$\frac{\langle U \rangle}{\bar{U}_m}$
η

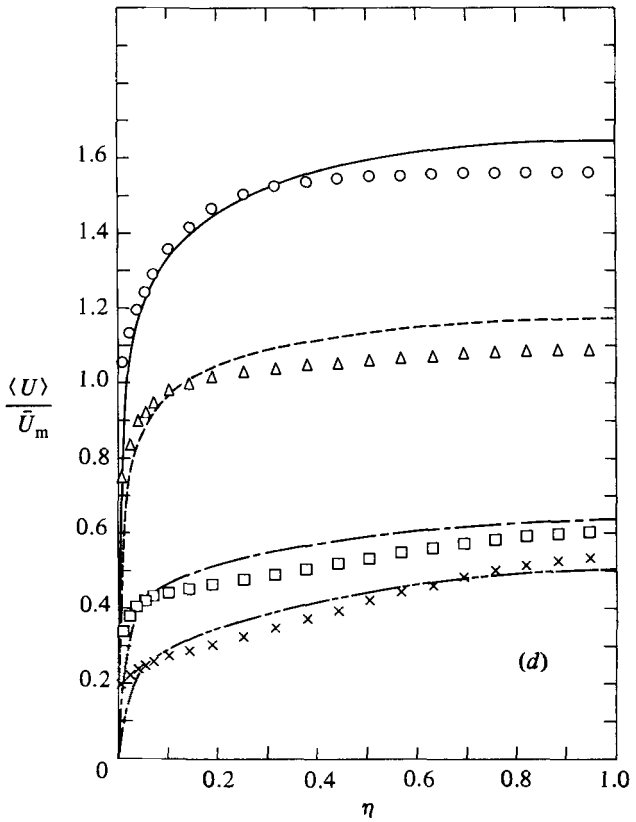

FIGURE 8. Ensemble-averaged velocity profiles at 3.6 Hz. (*a*) Decelerating period: ○, $\theta \approx 0°$; △, 45°; □, 90°; ×, 315°. (*b*) Accelerating period: ○, $\theta \approx 180°$; △, 225°; □, 270°; ×, 315°. Lines represent predictions. (*c*) Ensemble-averaged velocity profiles at 0.5 Hz; decelerating period; symbols as in (*a*). (*d*) Ensemble-averaged velocity profiles at 0.5 Hz; accelerating period; symbols as in (*b*).

velocity profiles in boundary-layer flows subjected to an adverse pressure gradient. These inflexion points have been observed also in other experiments on unsteady internal flows mentioned earlier.

Figure 8 also shows the comparison between the present experimental data and the predictions of the time-dependent calculation method. At 3.6 Hz (figures 8*a*, *b*), the predicted velocities during the entire cycle are slightly smaller than measurements in the central region while opposite results are observed for the wall region. At 0.5 Hz, the predicted velocities in the central region are smaller only in the phase interval $45° \lesssim \theta \lesssim 180°$. Near the wall the predicted values are always smaller than measured. It is also significant to note that calculations do not predict the experimentally observed inflexion profiles during any part of the cycle. Even after allowing for the possible errors in measurement near the wall, it can be said that the calculations are unable to predict correctly the variation of the velocity profiles with time at the lower oscillation frequency of 0.5 Hz. The apparently better prediction of the velocity profiles at the higher oscillation frequency is due to the confinement of oscillation effects to a relatively thin 'Stokes-like' layer at the high frequency. In fact, it can be expected that any turbulence model will produce good agreement in this region. This is because, at such a high frequency, turbulence modelling becomes less important in the core region where the inertia and pressure-gradient terms nearly

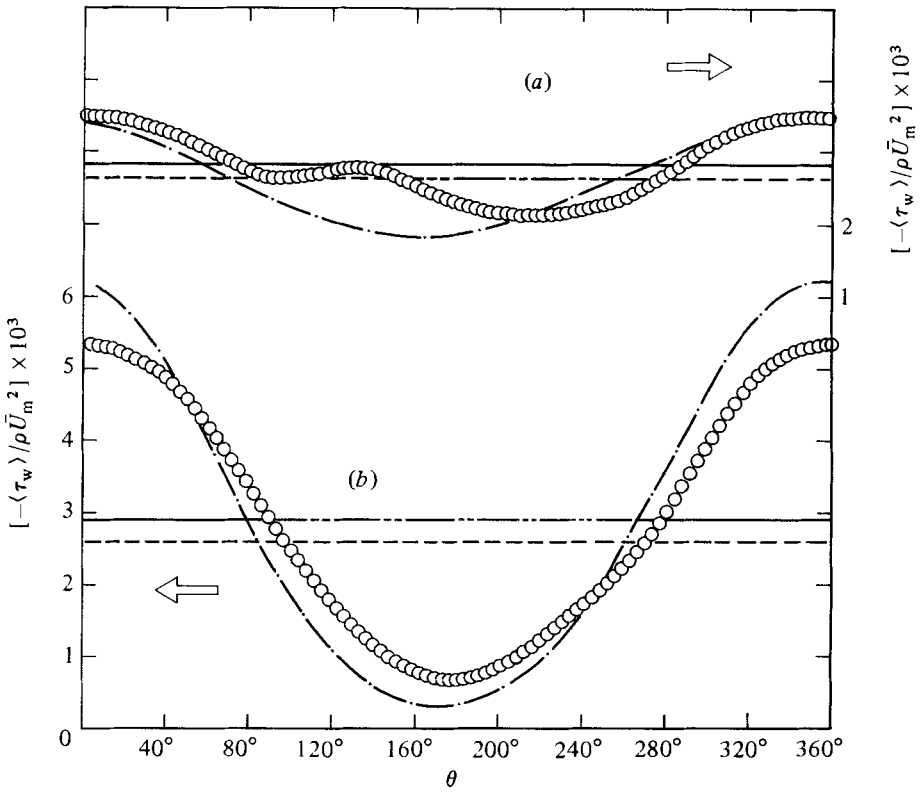

FIGURE 9. Phasewise variation of the ensemble-averaged wall shear stress; (*a*) 3.6 Hz; (*b*) 0.5 Hz: ○, experiment; —·—, prediction; ——, time mean of the experimental unsteady flow; ————, time mean of prediction and also time mean of quasi-stady flow, ----, steady flow at $\bar{R}e = 49400$. Note that some lines overlap.

balance each other while the shear term is practically negligible. At intermediate or lower frequencies, however, the shear-stress term plays a somewhat more significant role, and hence proper turbulence modelling is required for the correct prediction of the flow in the central part of the pipe also.

Near the wall, the influence of the shear stress is important at all frequencies, and this fact enhances the importance of using the correct model. In the present numerical model the eddy viscosity is scaled with the instantaneous turbulent kinetic energy and hence can vary with time. Since the dynamics of the turbulent structure is accounted for (to some extent), the present model is seen to perform reasonably well. However, the prediction is still not very accurate in the wall region, indicating the inadequacy of the modelling based on the quasi-steady assumption.

3.4.4. *Wall shear stress*

The measured wall-shear-stress variations at the two oscillation frequencies are shown in figure 9. The noticeable kink in the variation of $-\langle\tau_w\rangle$ at 3.6 Hz (figure 9*a*) is somewhat hard to explain. Since this kink does not occur at the minimum value, it cannot be attributed to the possible existence of backflow near the wall. Also, the minimum value is still considerably larger than zero, and no sign of reverse flow is indicated. In fact, this measurement was repeated several times taking all necessary precautions. The repetitions confirmed the accuracy of the measurement. The

variation of the turbulent intensity during the cycle, which was independently obtained from LDA measurements, also indicated the presence of such a kink. The time-mean value of the wall shear stress is found to be about 6 % higher than that of the corresponding quasi-steady flow of the same amplitude. This indicates that, at high frequencies, the time-mean velocity gradient at the wall is larger in the unsteady flow than in quasi-steady flow. This agrees with the authors' previous findings (Ramaprian & Tu 1980). If one combines this result with that of figure 5, namely that time-mean velocity is smaller than the quasi-steady value in the wall region, one is led to suspect that an inflexion point exists in the time-mean velocity profile very close to the wall. Such an inflexion point was indeed observed in the measurements of Ramaprian & Tu (1980). In that experiment, which was at a mean Reynolds number of 2100 and in which the oscillation frequency was 1.75 Hz, the inflexion point occurred sufficiently far from the wall, so that it could be detected directly by the LDA measurements. In the present study, the profile distortions at 3.6 Hz occur very much closer to the wall (at distances say of the order of 1 mm) because of the combination of higher Reynolds number and larger oscillation frequencies. In this region, LDA measurement are not very accurate. However, a study of figure 5 with the knowledge that measured velocities at the first two or three points nearest to the wall may in fact be even 'higher' than actual, will indicate the strong probability of an inflexion point in the velocity profile for the 3.6 Hz experiment. In any case, the independent wall-stress measurement indicates the existence of the inflexion point. At the oscillation frequency of 0.5 Hz (figure 9*b*), the phasewise variation of wall shear stress exhibits a slight distortion. This is a large-amplitude effect brought about by nonlinearity (power-law dependence of wall shear stress on velocity). The time-mean wall shear stress in unsteady flow, however, increases by less than 1 % relative to that of the corresponding quasi-steady flow, and hence the increase cannot be seen in the figure. It was already mentioned that the effect of oscillation on the time-mean velocity profile was also insignificant at this frequency. Since the effects on velocity and wall shear stress are both small, it is not possible to reach any conclusions regarding the existence or otherwise of an inflexion point in the time-mean velocity profile. It is very clear though that inflexion points are present in the ensemble-averaged velocity profiles.

Figures 9(*a*, *b*) also show the comparison between the measured wall shear stress and that predicted by the calculations. It is seen that the general trends are correctly predicted at each of the two oscillation frequencies. Quantitatively, however, discrepancies are observed. At 3.5 Hz, the measurements exhibit a kink as already mentioned and indicate a higher (by about 6 %) time-mean value than for quasi-steady flow. However, the predictions do not show any kink in the wall-shear-stress variation. Also, the predicted time-mean wall shear stress in unsteady flow is nearly equal to that in the quasi-steady flow. At 0.5 Hz the measured values are higher in the range of $45° < \theta < 240°$ and lower in the rest of the oscillation period compared with the predictions. The time-mean value of the measured wall shear stress is nearly equal (within 1 %) to that predicted. Both prediction and measurement of the time-mean wall shear stress agree approximately with the time-mean value in quasi-steady flow with an amplitude of 60 %. This value is much higher (by 15 %) than that for the corresponding steady flow at the mean Reynolds number. This is due to the amplitude effect already discussed in §3.3.2.

It is interesting to examine how the ensemble-averaged velocity in unsteady flow scales with the ensemble-averaged wall shear stress. Figure 10 shows the semilogarithmic plots of $\langle U \rangle$ in the wall-layer coordinates for several phase positions in the

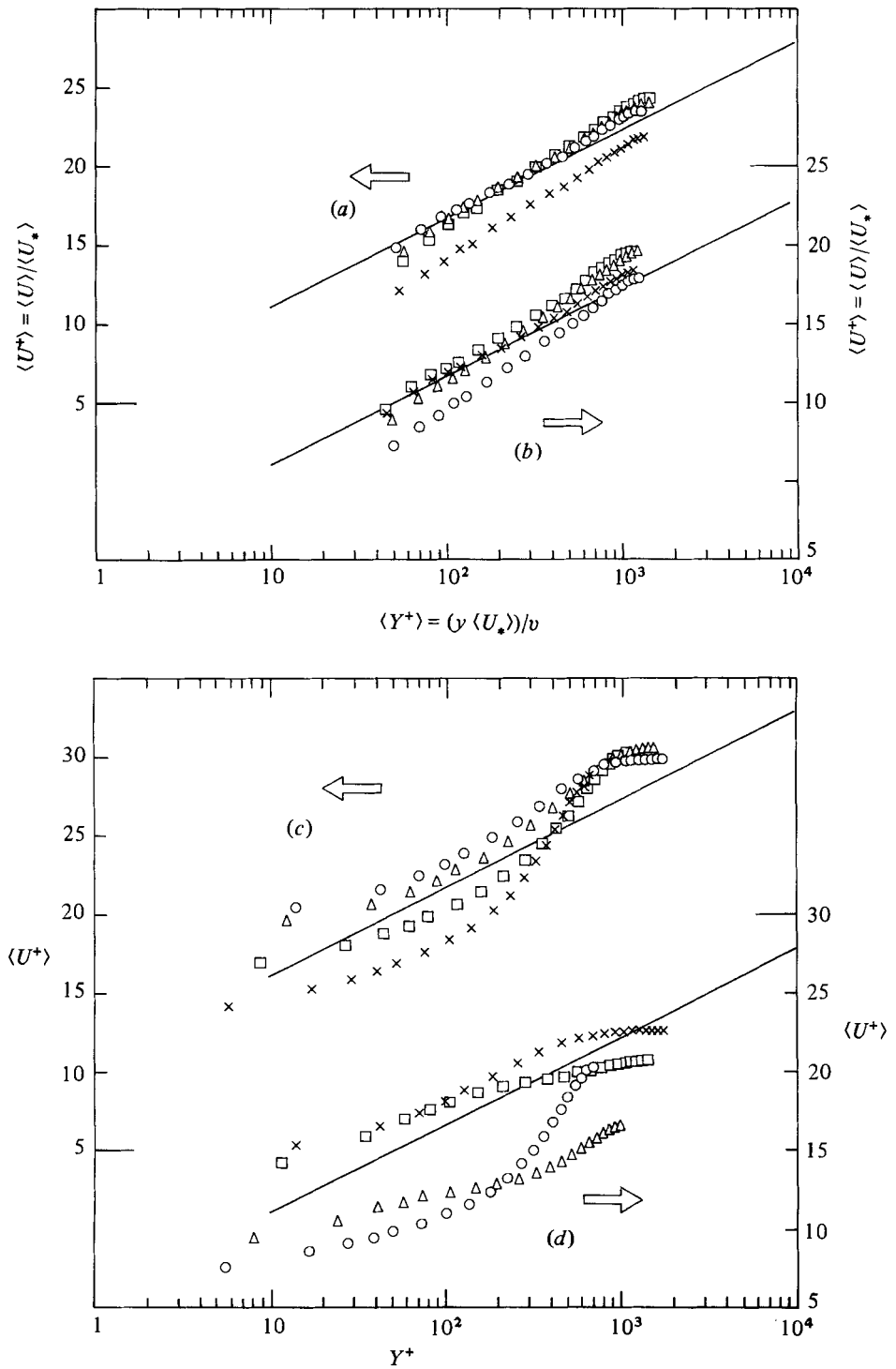

FIGURE 10. Ensemble-averaged velocity profile in the wall-layer coodinates; $f_{os} = 3.6$ Hz. (*a*) Decelerating period: ○, $\theta \approx 0°$; △, 45°; □, 90°; ×, 135°. (*b*) Accelerating period: ○, $\theta \approx 180°$; △, 225°; □, 270°; ×, 315°. ——, $U^+ = 2.44 \ln Y^+ + 5.5$. Ensemble-averaged velocity profile in the wall-layer coordinates; $f_{os} = 0.5$ Hz. (*c*) Decelerating period. (*d*) Accelerating period. Symbols as in (*a*) and (*b*).

oscillation cycle. Kinematic viscosity and ensemble-averaged wall shear stress are used in forming the wall-layer variables. Again, acceleration and deceleration regimes are shown separately for clarity. It is obvious that the velocity profiles do not follow a logarithmic law. This is not very surprising, since the velocity and wall shear stress experience different phase shifts. At 3.6 Hz, the departure from universal logarithmic law is strong during a part of the cycle. This part corresponds to the period in which the kink appears in the wall shear stress. Over the remainder of the cycle, the profiles seem to follow a logarithmic distribution though not the universal log law. This is due to the fact that the effect of the oscillation is confined to a thin layer at this frequency, and hence strong phase variations in velocity are confined to this layer. The flow in the rest of the pipe essentially performs a solid-body-like oscillation with no significant phase variations across this region. This will be seen more clearly from the phase-distribution plots discussed in Part 2. Thus the effect on each of the ensemble velocity distributions (in the wall-layer coordinates) across most of the pipe is that corresponding to the use of an inappropriate wall shear stress for obtaining the scaling velocity $\langle U_* \rangle$ and hence a change in the slope and intercept of the semilogarithmic line. This is indeed what is observed in figure 10(*a*). At an intermediate frequency the departure from the log law is even more drastic. Also, as seen from figures 10(*c*, *d*), the effect of oscillation extends over a large part of the pipe. There is a global distortion of the ensemble-averaged velocity profiles in wall-layer coordinates due to the varying phase shift between the local flow and the wall shear stress. The use of the wall shear stress as a scaling parameter loses all significance in this flow. It must be noted, however, that, if the frequency of oscillation is reduced to near-quasi-steady values, the ensemble-averaged velocity profiles can be expected to exhibit the universal log law.

Binder & Kueny (1981) reported that the ensemble-averaged velocity profiles in their experiment at high frequency of oscillation were found to follow the log law. This observation must be attributed to the difficulty of detecting small departures at the very small oscillation amplitude (5%) studied by them.

3.4.5. *Ensemble-averaged turbulence intensity*

The cross-sectional distributions of the ensemble-averaged turbulence intensity $u'_{\rm p}$ are shown in figure 11 for 8 phase positions in the cycle for each frequency studied. The time-mean turbulent intensity u' (in figure 6) is reproduced here again for ease of comparison. At high frequency (figures 11*a*, *b*) the ensemble-averaged turbulence-intensity variation is limited only to the region $\eta < 0.3$. It is seen clearly that the distribution of $u'_{\rm p}$ in the region $\eta > 0.3$ remains unchanged in time while the ensemble-averaged velocity pulsates, indicating a 'frozen structure'. This result is in agreement with the available data on periodic flows at high oscillation frequency. On the other hand, at the intermediate frequency of 0.5 Hz (figures 11*a*, *d*) the distributions vary significantly in shape all across the pipe, the profiles often crossing over one another at different locations. This indicates that the imposed unsteadiness spreads over the entire pipe cross-section. It may be noted that these crossovers will not occur in quasi-steady flow. The intensity of turbulence increases in the wall region with increase in the cross-sectional average velocity (that is during the acceleration part of the cycle), and decreases during the deceleration part of the cycle. However, the outer flow shows the opposite behaviour. It is thus seen that the flow in the central part of the pipe is least turbulent when the discharge is maximum. It is also seen that during a certain part of the cycle, say $\theta = 135°$–$225°$, the turbulence intensity has a maximum value in the neighbourhood of $\eta = 0.5$. Around the point of maximum

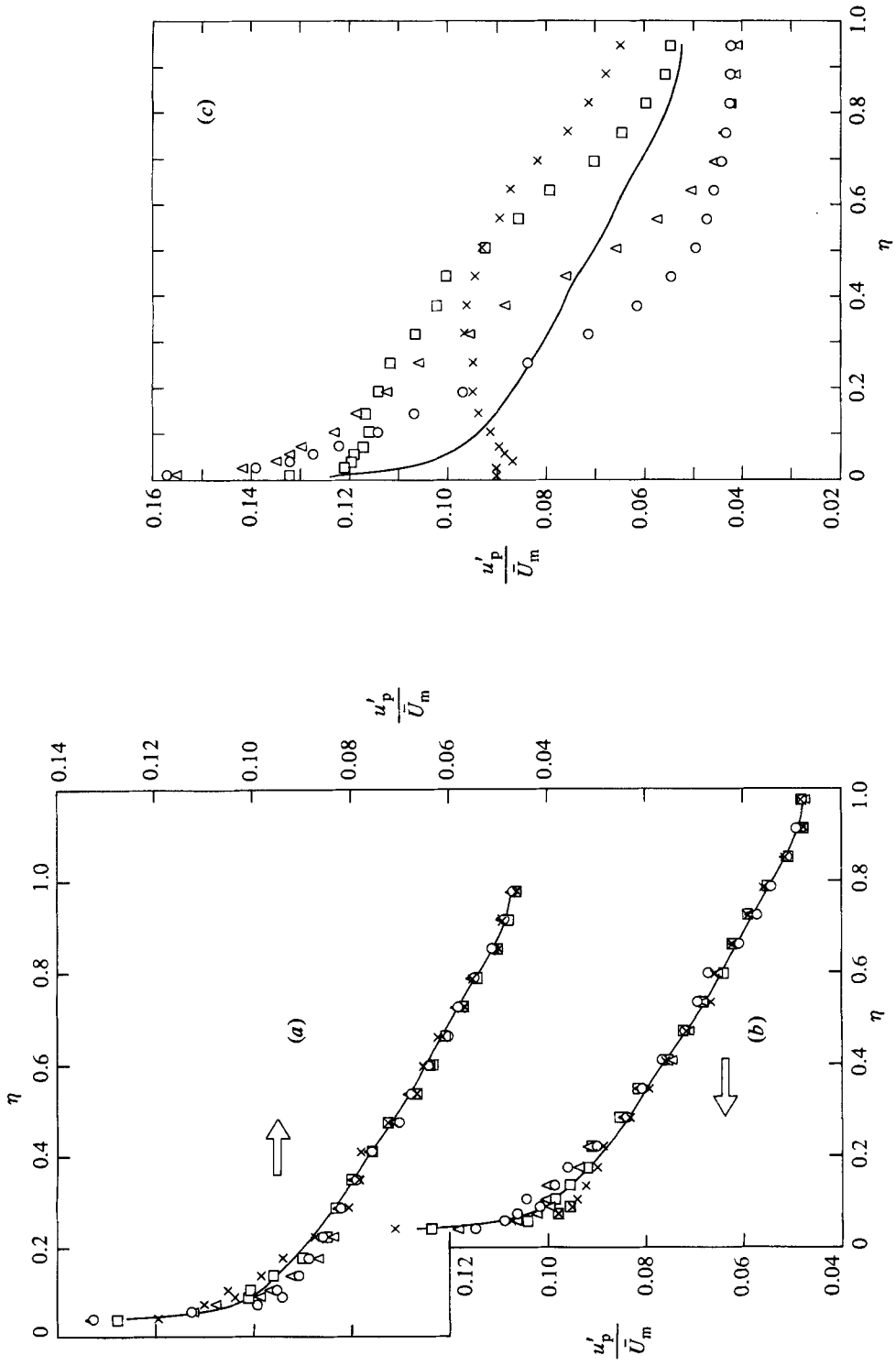
(a)
(b)
(c)
η
$\frac{u'_p}{\bar{U}_m}$
0.14
0.12
0.10
0.08
0.06
0.04
0.16
0.02
0
0.2
0.4
0.6
0.8
1.0

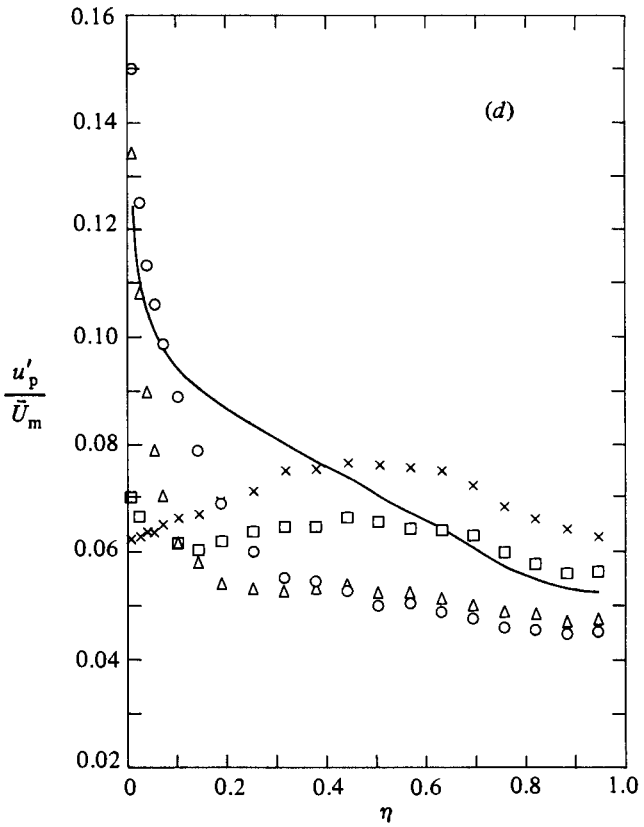

FIGURE 11. Ensemble-averaged longitudinal turbulent intensity distributions at $f_{os} = 3.6$ Hz. (*a*) Decelerating period. (*b*) Accelerating period. ——, time-mean distribution u'. Other symbols as in figures 10(*a*, *b*). (*c*) Ensemble-averaged longitudinal turbulent intensity distributions at $f_{os} = 0.5$ Hz. Decelerating period. ——, time-mean distribution u'. Other symbols as in figure 10(*a*). (*d*) Ensemble-averaged longitudinal turbulent intensity distributions at $f_{os} = 0.5$ Hz. Accelerating period. ——, time-mean distribution u'. Other symbols as in figure 10(*b*).

discharge the variation of u'_p across the pipe is a maximum, while around the point of minimum discharge the variation of u'_p across the pipe is a minimum. The ensemble distributions do not bear any resemblance either to the time-mean distribution or to the time-mean distribution in the quasi-steady flow (figure 6). In fact the crossing over of the u'_p profiles shows that the flow at 0.5 Hz does not even qualitatively behave like a quasi-steady flow.

Typical cross-plots of ensemble-averaged turbulent intensities showing the phase-wise distribution of u'_p are given for different locations across the pipe in figure 12. In figure 12(*a*), showing the results for 3.6 Hz, it can be seen that near the wall u'_p shows periodic variations. However, within a short distance from the wall the amplitude of variation of u'_p decreases, and eventually the distribution appears almost like a straight line, indicating very clearly the frozen structure of u'_p. It is also seen that u'_p shows large changes in phase as η increases, before attaining the frozen structure at larger values of η. On the other hand, at 0.5 Hz, the data for which are shown in figure 12(*b*), the cyclic variation of u'_p extends across the whole pipe. The large amplitude of variation is due to the large amplitude of velocity variation (64 %). It is also seen that near the wall the variation of u'_p is approximately sinusoidal with

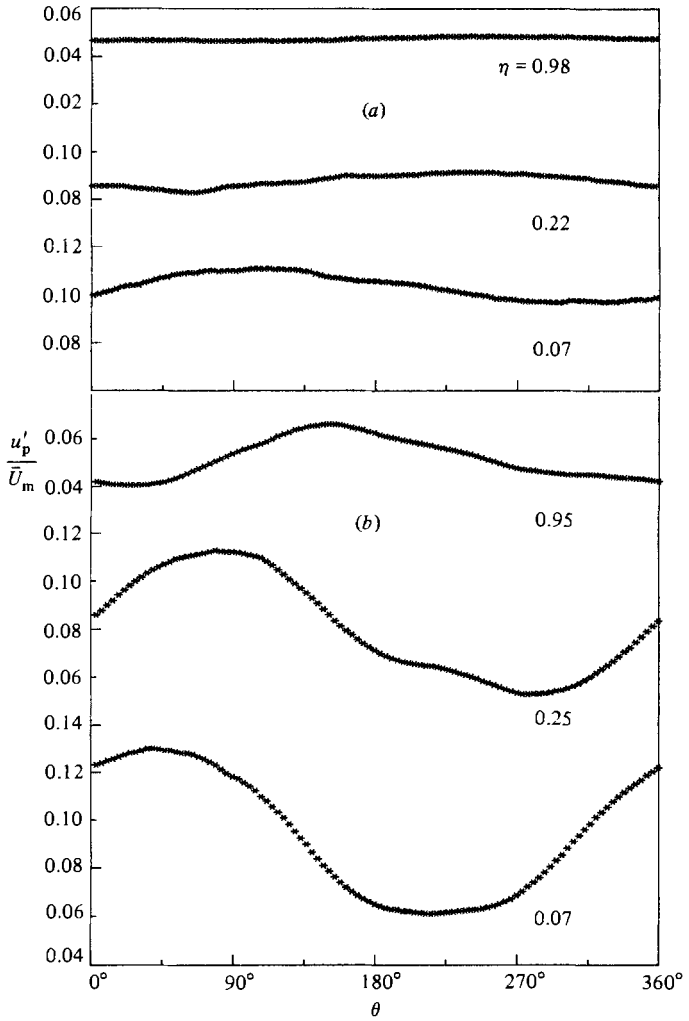

FIGURE 12. Phasewise distributions of ensemble-averaged longitudinal turbulent intensity: (*a*) $f_{os} = 3.6$ Hz; (*b*) $f_{os} = 0.5$ Hz.

a small phase lag with respect to the cross-sectional-average velocity. This phase lag increases with distance from the wall. At the same time, the profile gets more and more distorted with increase of distance from the wall. Kinks very similar to that observed in the wall-shear-stress variation at 3.6 Hz begin to appear in these profiles also. Finally, in the core region, the variation shows substantial distortion from a sine wave. In fact it is seen that u'_p remains practically constant at its minimum value over a significant part of the cycle. This part roughly corresponds to the interval $\theta = 270°$–$405°$. Thus the turbulent structure is by no means quasi-steady, even qualitatively. The present observations are generally in conformity with those of Mizushina *et al.* (1973, 1975). Both the investigations have clearly demonstrated that, at the frequencies studied, the turbulent structure cannot be associated with the corresponding ensemble-averaged velocity field in any simple manner.

3.4.6. *Ensemble-averaged Reynolds shear stress*

Figure 13 shows the Reynolds-shear-stress distribution across the pipe at various phase positions during the deceleration and acceleration periods of an oscillation

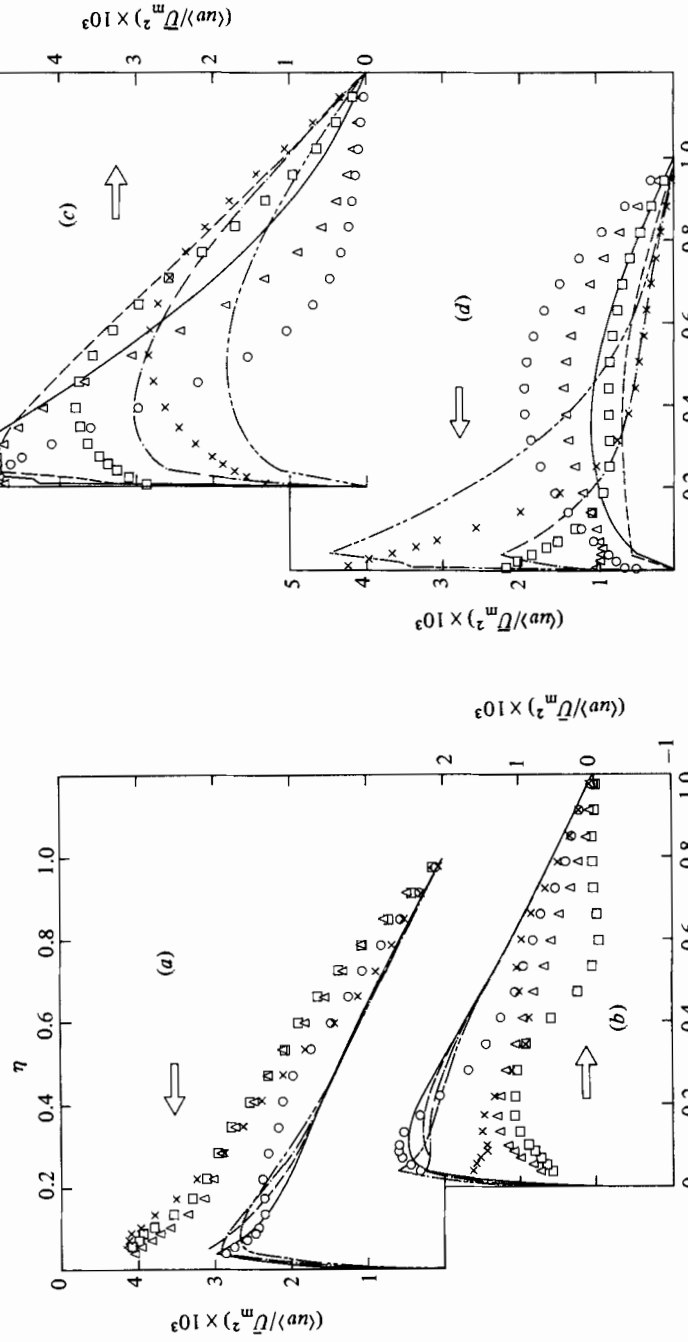

FIGURE 13. Ensemble-averaged Reynolds-shear-stress distributions and comparisons with predictions; $f_{os} = 3.6$ Hz. Symbols represent experimental data and lines represent predictions. (*a*) Deceleration period: ○, —, $\theta \approx 0°$; △, – – –, 45°; □, —·—, 90°; ×, — — —, 135°. (*b*) Acceleration period. ○, ——, $\theta \approx 180°$; △, — — —, 225°; □, —·—, 270°; ×, — — —, 315°: Ensemble-averaged Reynolds-shear-stress distributions and comparisons with predictions; $f_{os} = 0.5$ Hz. (*c*) Deceleration period. (*d*) Acceleration period. Symbols and lines as (*a*) and (*b*).

cycle. At the high frequency of 3.6 Hz, the Reynolds shear stress $\langle uv \rangle / \bar{U}_m^2$ near the wall varies widely (from about 5×10^{-4} at $\theta = 270°$ to about 40×10^{-4} at $\theta = 135°$). This can be compared with the variation from 25×10^{-4} to 35×10^{-4} of the wall shear stress $-\langle \tau_w \rangle / \rho \bar{U}_m^2$ (shown in figure 9). The large difference between the wall shear stress and the Reynolds shear stress near the wall is due to the large acceleration or retardation of the fluid. Owing to the phase difference between wall shear stress and the acceleration, the local shear stress in the near-wall region can be very different from the wall shear stress. The distributions of the ensemble-averaged shear stress across the pipe behave differently from those of the turbulence intensity u_p'. Predictions of the shear-stress distributions are also shown in these figures. It is seen that calculation indicates a small amplitude of fluctuation of the shear stress near the wall ($\eta < 0.4$) and practically a frozen structure in the core region.

A study of the results for the 0.5 Hz experiments shown in figures 13 (*c*, *d*) indicates large variations of the shear-stress distribution all across the pipe. The shear-stress data are expected to be far more accurate for this experiment than at the higher frequency. The large amplitude of the shear stress is of course to be expected in view of the large amplitude of flow modulation in this case. Again, crossover profiles similar to those of u_p' are observed in these figures also. In other words, large values of shear stress near the wall are associated with small values in the outer region and *vice versa*. Complete departure of the turbulence structure from that of the quasi-steady flow is obvious. Numerical predictions of this flow are also shown in the figures for comparison. Again large quantitative differences can be observed between prediction and experiment, with the model being able to predict only general trends.

A better comparison between the predicted and measured structure of the turbulent shear stress as well as a better understanding of the behaviour of the shear stress is provided by the typical cross-plots of Reynolds-shear-stress distribution shown in figure 14. From figure 14 (*a*), corresponding to 3.6 Hz, it can be easily seen that the numerical model fails to capture the details of the shear-stress variation over the cycle, even though it seems to predict the average value for the cycle reasonably well. At the lower frequency of 0.5 Hz the model seems to predict the variations of the shear stress reasonably well, although with a phase shift. In fact, the apparent poor performance of the calculation in figure 13 (*b*) is now seen to be essentially caused by a phase difference between prediction and measurement. It thus appears that the quasi-steady model, which can predict the periodic flow very well at very low frequencies, is unable to follow the changes during the cycle as the oscillation frequency reaches moderately large values. Eventually, at high frequencies, the model breaks down completely and indicates a frozen structure during the entire cycle.

Figure 14 also indicates very clearly that kinks begin to develop in the phasewise distributions of the measured Reynolds stress at both the frequencies. These kinks resemble those observed in the wall shear stress and turbulence intensity distributions. These are presumably due to the nonlinear interaction between the turbulent structure and the imposed oscillations. This interaction seems to be present even at 0.5 Hz.

4. Conclusions

The results presented so far for fully developed periodic pipe flow at Reynolds number of 50000 have further confirmed the conclusions of the earlier work of Ramaprian & Tu (1980) on similar flows at transitional Reynolds numbers that the time-mean flow in the pipe is indeed affected by imposed oscillation when the

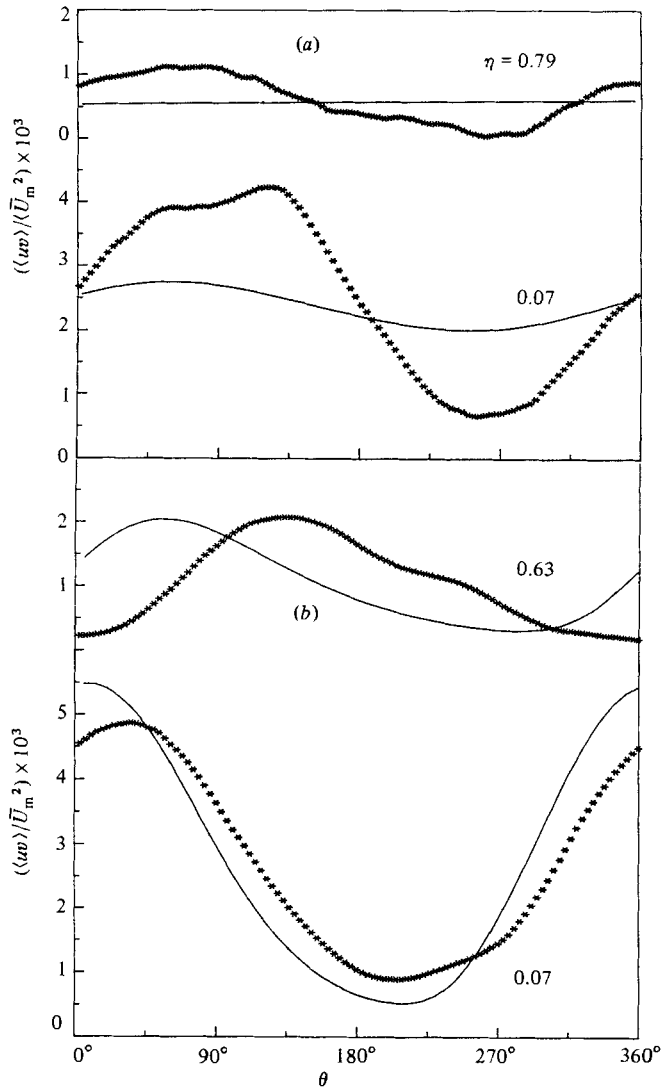

FIGURE 14. Phasewise distributions of the Reynolds shear stress and comparison with predictions: (*a*) $f_{os} = 3.6$ Hz; (*b*) $f_{os} = 0.5$ Hz; *, experiment; ——, prediction.

oscillation frequency approaches the characteristic frequency of turbulence. The present velocity and wall-shear-stress data also suggest the existence of an inflexion point in the time-mean velocity profile very near the wall. Further, neither the time-mean nor the ensemble-averaged velocity follows the universal log law at the frequencies studied. At the lower frequency studied, the ensemble-averaged velocity exhibits strongly distorted profiles with inflexion points. At the higher frequency, this distortion is confined to a thin region near the wall, and the rest of the distribution is smooth. The ensemble-averaged turbulence intensity u'_p and Reynolds shear stress $\langle uv\rangle$ are also significantly affected by unsteadiness. At the lower frequency these profiles are considerably distorted. The turbulent intensity remains 'frozen' at a low value over nearly half the cycle at this frequency. At the higher frequency the turbulence intensity remains frozen throughout the cycle. Calculations using a

quasi-steady turbulence model such as the Prandtl-energy model predict negligible effect of unsteadiness on the time-mean flow. Further, the method is unable to follow the detailed turbulence history through the cycle even at the lower frequency, and, in fact, completely breaks down at the higher frequency. However, the prediction of the ensemble-averaged flow, especially in the outer region, improves at the high frequency. This is simply because of the negligible role played by turbulence in this flow.

This study was supported by the U.S. Army Research Office Grant DAAG-29-79-G-0017, and the authors gratefully acknowledge this support.

REFERENCES

ACHARYA, M. & REYNOLDS, W. C. 1975 Measurements and predictions of a fully developed turbulent channel flow with imposed controlled oscillations. *Stanford Univ. Thermosci. Div. Tech. Rep.* TF-8.

BINDER, B. & KUENY, J. L. 1981 Measurements of the periodic velocity oscillations near the wall in unsteady turbulent channel flow. In *Unsteady Turbulent Shear Flows* (ed. R. Michel, J. Cousteix & R. Houdeville), pp. 100–108. Springer.

COUSTEIX, J., HOUDEVILLE, R. & JAVELLE, J. 1981 Response of a turbulent boundary layer to a pulsation of the external flow with and without adverse pressure gradient. In *Unsteady Turbulent Shear Flows* (ed. R. Michel, J. Cousteix & R. Houdeville), pp. 120–144. Springer.

KIRMSE, R. E. 1979 Investigations of pulsating turbulent pipe flow. *ASME Paper* 79-WA/FE-1.

KITA, Y., ADACHI, Y. & HIROSE, K. 1980 Periodically oscillating turbulent flow in a pipe. *Bull. JSME* **23**, 656–664.

LAUFER, J. 1954 The structure of turbulence in fully developed pipe flow. *NACA Rep.* 1174, pp. 407–434.

MIZUSHINA, T., MARUYAMA, T. & HIRASAWA, H. 1975 Structure of the turbulence in pulsating pipe flows. *J. Chem. Engng Japan* **8**, 210–216.

MIZUSHINA, T., MARUYAMA, T. & SHIOZAKI, Y. 1973 Pulsating turbulent flow in a tube. *J. Chem. Engng Japan* **6**, 487–494.

OHMI, M., USUI, T., TANAKA, O. & TOYAMA, M. 1976 Pressure and velocity distribution in pulsating turbulent pipe flow. *Bull. JSME* **19**, 951–957.

OHMI, M., KYOMEN, S. & USUI, T. 1978 Analysis of velocity distribution in pulsating turbulent pipe flow with time-dependent friction velocity. *Bull. JSME* **21**, 1137–1143.

PATANKAR, S. V. 1967 Heat and mass transfer in turbulent boundary layers. Ph.D. thesis, Imperial College of Science and Technology, Mech. Engng Dept.

RAMAPRIAN, B. R. & TU, S. W. 1980 An experimental study of oscillatory pipe flow at transitional Reynolds numbers. *J. Fluid Mech.* **100**, 513–544.

RAMAPRIAN, B. R. & TU, S. W. 1982 Study of periodic turbulent pipe flow. *IIHR Rep.* 238, *Iowa Inst. Hydraul. Res.*

RAMAPRIAN, B. R. & TU, S. W. 1983 Fully developed periodic turbulent pipe flow. Part 2. The detailed structure of the flow. *J. Fluid Mech.* **137**, 59–81.

RAO, K. N., NARASIMHA, R. & BADRI NARAYANAN, M. A. 1971 The 'bursting' phenomena in a turbulent boundary layer. *J. Fluid Mech.* **48**, 339–352.

VASILIEV, O. F. & KVON, V. I. 1971 Friction forces of unsteady flows in open channels and pipes. In *Proc. 14th Congress of IAHR, Paris*, vol. 2, pp. B 23.1–23.10.